J Fluoresc (2011) 21:983–989
DOI 10.1007/s10895-010-0684-3

ORIGINAL PAPER

# Confocal Fluorescence Detected Linear Dichroism Imaging of Isolated Human Amyloid Fibrils. Role of Supercoiling

**Gábor Steinbach · István Pomozi · Dávid Péter Jánosa · Josef Makovitzky · Győző Garab**

Received: 5 January 2010 / Accepted: 1 June 2010 / Published online: 17 June 2010


**Abstract** Amyloids are highly organized insoluble protein aggregates that are associated with a large variety of degenerative diseases. In this work, we investigated the anisotropic architecture of isolated human amyloid samples stained with Congo Red. This was performed by fluorescence detected linear dichroism (FDLD) imaging in a laser scanning confocal microscope that was equipped with a differential polarization attachment using high frequency modulation of the polarization state of the laser beam and a demodulation circuit. Two- and three-dimensional FDLD images of amyloids provided information on the orientation of the electric transition dipoles of the intercalated Congo Red molecules with unprecedented precision and spatial resolution. We show that, in accordance with linear dichroism imaging (Jin et al. Proc Natl Acad Sci USA 100:15294, 2003), amyloids exhibit strong anisotropy with preferential orientation of the dye molecules along the fibrils; estimations on the orientation angle, of around 45°, are given using a model calculation which takes into account the helical organization of the filaments and fibrils. Our data also show that FDLD images display large inhomogeneities, high local values with alternating signs and, in some regions, well identifiable μm-sized periodicities. These features of the anisotropic architecture are accounted for by supercoiling of helically organized amyloid fibrils.

**Keywords** Amyloid · Anisotropy · Fluorescence detected linear dichroism · Laser scanning confocal microscopy · Supercoiling

**Electronic supplementary material** The online version of this article (doi:10.1007/s10895-010-0684-3) contains supplementary material, which is available to authorized users.

G. Steinbach · I. Pomozi · D. P. Jánosa · G. Garab (✉)
Biological Research Center,
Hungarian Academy of Sciences,
P.O. Box 521, Szeged 6701, Hungary
e-mail: gyozo@brc.hu

I. Pomozi
Pi Vision Bt.,
Budapest, Hungary

J. Makovitzky
Department of Neuropathology,
University of Heidelberg,
Heidelberg, Germany

G. Garab
Medicopt Bt.,
Szeged, Hungary

## Introduction

Amyloids are highly ordered insoluble fibrous protein aggregates. They are deposited in a wide range of tissues and are associated with neurodegenerative diseases and a number of other pathological conditions [1–3]. Amyloids are also in the focus of interest with regard to the mechanisms of protein folding and misfolding and their correlations with fundamental biological functions and cellular dysfunctions, respectively [4]. For material sciences, the fact that they can self-assemble from simple building blocks, such as peptides and proteins, holds the promise of the creation of intelligent and highly stabile nanomaterials [5, 6]. Hence, the formation, structure and elasticity of these hierarchically organized macro-assemblies, at different levels of complexity, are of crucial importance not only for the diagnosis and prevention of diseases but also for basic biology as well as for nanotechnology.

The formation of amyloids is initiated by the aggregation of unfolded or partially unfolded proteins. These aggregates assemble into protofibrils or protofilaments and then to mature fibrils, which are deposited in large, microscopic

patches or plaques. [4, 7] The core structure of amyloids, the so-called cross-β structure, is composed of β-sheets with strands running perpendicular to the axis of the fibrils [8, 9]; they are assembled in polymorphic and stepwise manner. [10–12] In many amyloids the fibrils have been shown to be composed of a double helix of two protofilament pairs wound around a hollow core. [13] Paired helical filaments (PHFs) have been observed [14–17] with diameters of 5–20 nm and periodicities typically between 75 and 160 nm [17, 18]. Helical structures, 'double tracked' ribbon-like entities wound around the non-protein components of AA amyloids, have also been identified on cryofixed and freeze-substituted samples [19]. Plaques of microscopic sizes also exhibit a high level order, as shown by their inherent and dye-enhanced birefringence as well as metachromasia and anisotropic effects, originating from the ordered packing of the protein components in the fibrils [1] as well as from other, non-fibrillar constituents [20]. Hence, amyloids appear to be highly organized at all levels of their structural hierarchy. This is documented by a wide arsenal of methods of structure investigations, including atomic force, electron and light microscopy techniques and X-ray and optical diffraction, and a range of optical spectroscopic tools, from the far UV to the infrared, as well as magnetic resonance spectroscopic methods [7, 8, 13, 21–26]. Nevertheless, because of the complexity of virtually all amyloid structures and the presence of disorders and inhomogeneities, our understanding of their self-assembly, structure and elasticity are still far from being complete, and further methods, which provide specific information on their molecular organization, are of interest.

For many decades, birefringence of Congo Red stained tissues served for the diagnosis of amyloidosis, and was also used for the identification of amyloids in vitro. Birefringence is given rise by the anisotropic protein architecture of amyloid deposits [1, 27]. By using polarization microscopy, the molecular order was detected also for the endogenous sugars and other "non-protein" compounds, which cooperatively participate, in highly oriented fashion, in the assembly of the amyloid fibrils [20, 28, 29]. An advanced imaging technique, linear dichroism (LD) imaging confirmed that the molecular architectures of amyloids are indeed highly anisotropic [30]. In contrast to the birefringence, which is difficult to quantify in terms of anisotropic molecular architecture, the imaging of LD provides specific and quantitative information on the orientation of the electric dipole transition moment of Congo Red, which was found to be oriented preferentially along the long fiber axis [30]. These LD measurements were carried out on a microscope equipped with rotating polarizers and a digital camera. The spatial resolution and the precision of measurements of anisotropy can be further improved by confocal microscopy and high frequency modulation/demodulation techniques, as applied first for a scanning stage microscope [31], and more recently on a laser scanning microscope (LSM) [32]. Our DP-LSM (differential-polarization laser scanning microscope) allows the rapid and precise microscopic determination of the main differential-polarization quantities [33]. In this work, we imaged FDLD of isolated human amyloids stained with Congo Red. FDLD, the fluorescence detected linear dichroism, as LD, originates from non-random distribution of the absorbance dipoles; however, FDLD is calculated from the intensity difference between the fluorescence emissions elicited by the two orthogonally polarized beams, instead of measuring directly the absorbance difference between the two beams. In confocal regime, this technique offers superior spatial resolution and high precision data [34]. Our measurements show that amyloids exhibit strong anisotropy, and confirm the preferentially parallel orientation of the transition dipoles of Congo Red with respect to the long axis of the fibrils, with a calculated intercalation angle of around 45°. However, our measurements also reveal characteristic anisotropic patterns, domains with alternating signs and, in some samples, well discernible periodicities, macro-organization features that are accounted for by supercoiling of helically organized fibrils. The results have been presented in a preliminary form [35].

## Experimental

The preparation of amyloid fibrils was performed according to [36, 37]. The slides were prepared as described earlier [38, 39]. The sections were stained with freshly prepared 0.1% aqueous Congo Red solution (Merck, Darmstadt, Germany) according to [40], for 10 min and, after rinsing in running water (30 min), were mounted with diluted gum arabic ("Kristall-Gummi" Gutenberg, Mainz, Germany) solution [41].

Confocal fluorescence intensity images were recorded on a Zeiss LSM410 laser scanning microscope. Samples stained with Congo Red were excited at 488 nm and the fluorescence emissions were observed above 560 nm. Confocal FDLD images were recorded on the same LSM, equipped with a differential-polarization (DP) attachment [32–34]. Briefly, a DP attachment, which modulated the polarization state of the exciting laser beam at 100 kHz, using a photoelastic modulator (PEM-90, Hinds Instruments), was placed between the beam expander and the main beam splitter. The signal, proportional to the fluorescence intensity difference was obtained from the demodulation circuit.

The magnitude of FDLD was calculated as the difference in fluorescence intensities associated with the absorbances for the two orthogonally polarized beams; when related to

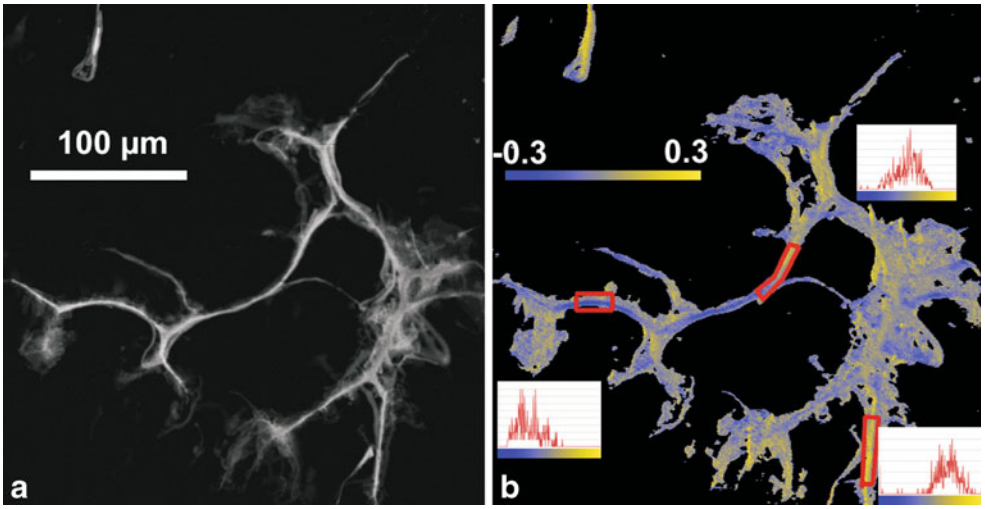


**Fig. 1** Confocal fluorescence intensity (**a**) and fluorescence detected linear dichroism (FDLD) (**b**) images of isolated human amyloid fibrils stained with Congo Red. The excitation wavelength was 488 nm, the fluorescence emission was detected above 560 nm. The *color code* in **b** indicates the magnitude of orientation parameter ($S=FDLD/3I_a$, where $I_a$ is the average fluorescence intensity). Insets in B, histograms of S values in the framed areas

the total intensity, the $S$ orientation parameter was obtained: $S=\Delta I/3I_a$ for small $\Delta I$, where $\Delta I$ corresponds to the intensity difference in the fluorescence emissions elicited by the two orthogonally polarized beams, and $I_a$ to the average fluorescence intensity, calculated from the sum of the two intensities elicited by the two orthogonally polarized beams. $S$ can be used for calculating the orientation angle [42], see also [34]; this signal was stored and displayed by the computer of the LSM.

## Results and discussion

LD imaging on amyloids was first applied by Jin et al. [30], who used a microscope equipped with a rotating polarizer and a camera detection. With the use of this technique, which provides unique information on the orientation of the electric transition dipoles with respect to a coordinate system fixed to the sample, the authors have concluded that Congo Red molecules are aligned along the fiber axis. The DP-LSM assembled in our laboratory, using high frequency modulation of the laser beam and demodulation of the signal of the photomultiplier detecting the transmitted light, allows pixel by pixel LD imaging. However, the set-up is also suited to measure LD via fluorescence detection. In this regime, instead of measuring the absorbance difference (LD) for the two orthogonally polarized beams, we measure FDLD, the intensity difference of the fluorescence emissions elicited by the two beams. One advantage is that this detection technique measures the true absorbance, and scattering artifacts are eliminated. In addition, fluorescence detection has high sensitivity, which can be important for weakly absorbing samples. However, the main advantage of the fluorescence detection is that it is ideally suited for confocal laser scanning microscopes, most of which allow confocal imaging in fluorescence rather than in transmission mode. Hence, FDLD can offer not only better sensitivity but also superior spatial resolution.

As seen in Fig. 1, amyloids exhibit strong FDLD signals, which evidently carry independent information from the fluorescence intensity signals. Although the anisotropy pattern appears to be more complex than anticipated (see below), it is clear that the FDLD signals tend to follow the alignment of the fibrils: they tend to display positive FDLD signal for fibrils aligned vertically and negative FDLD signals for horizontally aligned sections (see also the 3D reconstructed FDLD image—Supplemental Material). This can be confirmed and quantified by the histograms of well aligned sections of the fibrils (inset Fig. 1b). Histograms on vertically and horizontally aligned fibrillar sections, which exhibit strong dichroisms, revealed that the mean values of $S$ were symmetrical, −0.16±0.06 and 0.14±0.06, for horizontally and vertically aligned fibrils, respectively; whereas the sections at 45º displayed nearly zero dichroism, as expected.

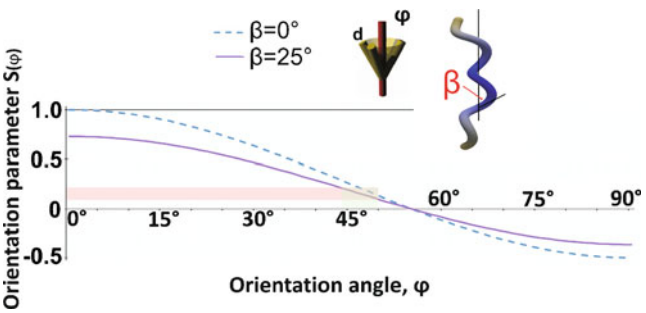


**Fig. 2** Dependence of the orientation parameter, S, on the orientation angle, φ, of the electric transition dipole vector (**d**) of Congo Red with respect to the protein scaffold of the amyloid fibrils for rod (*dashed line*, β=0°) and the helical model with a tilt angle of β=25° (*solid line*)—based on the parameters published by Ferrari et al. [17]. Insets, the geometries used in the model

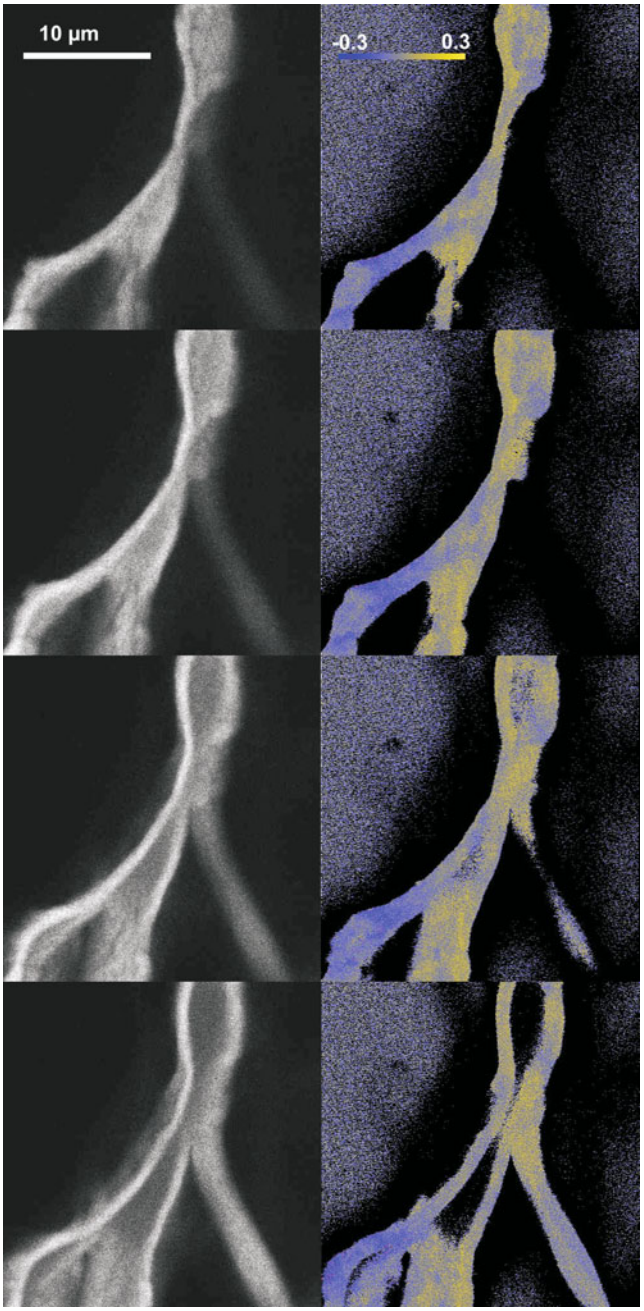


**Fig. 3** Series of confocal fluorescence intensity (*left panel*) and FDLD (*right panel*) images of an amyloid sample stained with Congo Red. Z-distances between the optical slices, 1 µm. The excitation wavelength was 488 nm, the fluorescence emission was detected above 560 nm. The *color code* indicates the magnitude of the orientation parameter S

These data are in harmony with the conclusion of [30] concerning the preferential orientation of the transition dipole vector of Congo Red—along the long axis of the fibrils.

Based on the measured FDLD data, model calculations can be performed to calculate the value of the φ orientation angle between the transition dipole vector of Congo Red and the long axis of the fibrils. When using the simplest

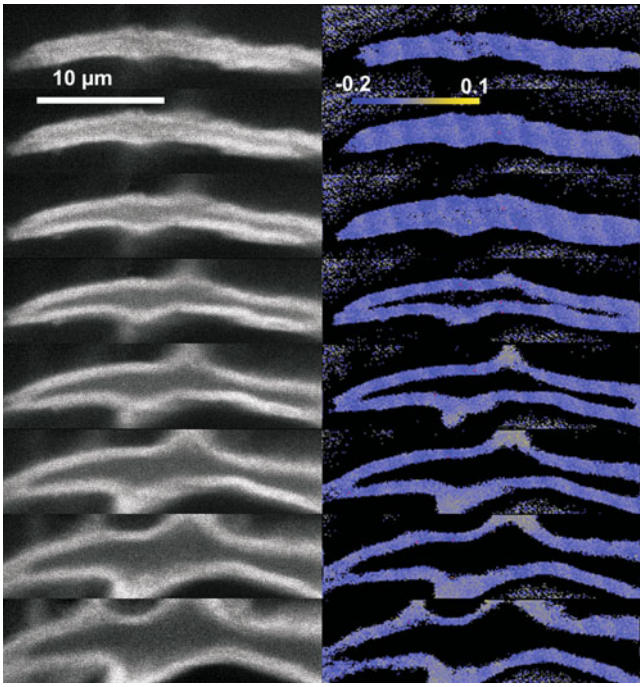


**Fig. 4** Series of optical sections of isolated human amyloid sample stained with Congo Red; Z-distances between the optical slices, 1 µm. *Left panel*, fluorescence intensity images; right panel, FDLD images with a *color code* indicating the magnitude of S, the orientation parameter

model of the fibril, a rod, the average φ orientation angle of the dye molecule, calculated from the average S values of well aligned fibrillar bundles, is found at around 49° and when taking into account the statistically significant higher S values of 0.2, we obtain 47° (Fig. 2). For a more complicated model, such as the PHF model, which takes into account the helical organization of the filaments, φ must assume smaller values because of the helical tilt of the filaments. The fact that induced CD signals are obtained upon the binding of Congo Red to amyloid fibrils and fibrillar proteins but not to unfolded polypeptides [43] is in

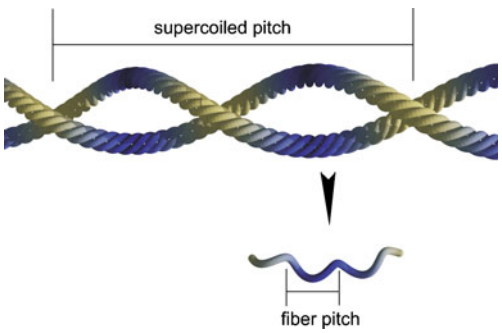


**Fig. 5** A 3D geometrical model illustrating that a supercoiling of helical structures via slithering can give rise to anisotropic macro-assemblies with a higher level periodicity; the figure also shows the sizes of the helices in relation to the color-coded FDLD signal, which would be associated with such a periodic structure

harmony with the notion that this dye is binding to the protein scaffold of amyloids, where it forms (a) helical array(s).

The helical organization of the filaments and protofibrils [7] is taken into account in the following manner. When the dye is bound to the protein which is then assembled into a helix with tilt angle β, the dipole orientation will vary in an angular interval of fluctuation that is determined by β. This 'precession' of the dipole along the helix can be taken into account as in the model published earlier [42, 44]. Conversely, the determination of the orientation angle, φ, with respect to the protein scaffold from the FDLD measurements depends also on the helical parameters. The tilt angle of the helix can be calculated from the structural parameters obtained from electron microscopy: with a width of 20 nm and a periodicity of 130–160 nm [17] the tilt angle is found between about 22° and 26°. With a tilt angle of 25° and the values of S=0.14±0.06, calculated from the measured FDLD, we obtain φ angles between 44° and 50° (Fig. 2); the lower value belongs to the statistically significant strongest FDLD.

Upon a closer inspection of the FDLD images it can be seen that the anisotropy in the amyloid samples cannot be interpreted in simple terms of their filamentous structure. With the rare exception of areas with no apparent local variations in the sign and magnitude of FDLD, most areas contain large inhomogeneities. These inhomogeneities show no correlation with intensity variations in the fluorescence, and thus cannot be accounted e.g. for by staining inhomogeneities. The presence of inhomogeneities can be recognized already at low magnification (Fig. 1) but can be more clearly seen in higher magnification images, such as shown in Fig. 3. Again, it is clear that while the fluorescence intensity images do not show any domain organization the FDLD images display large local variations (Fig. 3, right panel). In most areas of about 2 μm× 2 μm both FDLD signs occur, albeit not with the same magnitude. There are regions with clear dominance of one or the other orientations. In other regions, the FDLD, if averaged for the given area, corresponding to lower spatial resolution, would easily vanish or be largely diminished. The local variations in the images most probably reflect alignment-variations of the fibrils due to their macro-organization in the deposits. Hence, the presence of twisted structures and the exposure of certain fibril-alignments in the amyloid deposits, which often contain fibrils with different orientations, readily explain our observations.

In some samples the local variations in the FDLD displayed a clearly recognizable periodicity, while no such pattern was present in the fluorescence images (Fig. 4). The periodicity, determined by fast Fourier analysis was found between 1.48 and 1.74, with a mean value of 1.57±0.1, obtained from 5 independent determinations on the second, third and fourth sections in Fig. 4. This kind of anisotropy evidently originates from a macro-helical organization of the fibrils (Fig. 5). Such structures can self-assemble by supercoiling from lower level helically organized structural elements.

Typical examples of superhelical structure with long-range order are nuclei and other DNA condensates, which spontaneously supercoil into compact structures exhibiting chirally organized macro-assemblies [45–47]. Via supercoiling of helical structures the packing density can be dramatically increased, which also significantly contributes to the structural stability of the supercoiled molecular macroassemblies (e.g. [48]). Supercoiling can result in typical macro-structures, such as characterized by branch collision and slithering [49]. These structures exhibit higher level periodic or quasi-periodic structures. Figure 5 schematically shows that a lower level helical structure, with a pitch of unity can assemble into a higher level structure with a much larger pitch and a periodicity in its anisotropy. For amyloids, PHFs possess a pitch of about 150 nm, which might assemble in supercoiled structures with a pitch of about 3 μm and a periodicity of 1.5 μm. With branch collision [49] the helical filaments can form less regular but still highly anisotropic structures, i.e., assemblies in which relatively large sections of the filaments assume a clear tendency in their alignment (e.g. aligned vertically), while the filaments might be continued in sections with nearly orthogonal alignments. This kind of superhelical structures readily explain the presence of large inhomogeneities and highly anisotropic domains with alternating signs, and even periodicities in FDLD, which are absent in the fluorescence intensity images. It is proposed, on analogy with DNA condensates, that supercoiling significantly contributes to the stability of amyloid deposits. In order to obtain further details on the macro-organization of amyloids and their structural stability and flexibility, it would be necessary to carry out a more complete polarimetric imaging [50] of amyloid deposits under different experimental conditions.

## References

1. Sipe JD, Cohen AS (2000) Review: history of the amyloid fibril. J Struct Biol 130(2–3):88–98
2. Kelly JW (1998) The alternative conformations of amyloidogenic proteins and their multi-step assembly pathways. Curr Opin Struct Biol 8(1):101–106
3. Chiti F, Dobson C (2006) Protein misfolding, functional amyloid, and human disease. Annu Rev Biochem 75:333–366
4. Dobson CM (2003) Protein folding and misfolding. Nature 426 (6968):884–890
5. Makabe K, Biancalana M, Yan S, Tereshko V, Gawlak G, Miller-Auer H, Meredith SC, Koide S (2008) High-resolution structure of a self-assembly-competent form of a hydrophobic peptide captured in a soluble beta-sheet scaffold. J Mol Biol 378(2):459–467

6. Karsai A, Martonfalvi Z, Nagy A, Grama L, Penke B, Kellermayer MSZ (2006) Mechanical manipulation of Alzheimer's amyloid beta 1–42 fibrils. J Struct Biol 155(2):316–326
7. Giurleo JT, He X, Talaga DS (2008) β-Lactoglobulin assembles into amyloid through sequential aggregated intermediates. J Mol Biol 381(5):1332–1348
8. Sunde M, Serpell LC, Bartlam M, Fraser PE, Pepys MB, Blake CCF (1997) The common core structure of amyloid fibrils by synchrotron X-ray diffraction. J Mol Biol 273(3):729–739
9. Blake C, Serpell LC (1996) Synchrotron X-ray studies suggest that the core of the transthyretin amyloid fibril is a continuous beta-sheet helix. Structure 4(8):989–998
10. Kodali R, Wetzel R (2007) Polymorphism in the intermediates and products of amyloid assembly. Curr Opin Struct Biol 17(1):48–57
11. Kellermayer MSZ, Karsai A, Benke M, Soos K, Penke B (2008) Stepwise dynamics of epitaxially growing single amyloid fibrils. Proc Natl Acad Sci USA 105(1):141–144
12. Celej MS, Caarls W, Demchenko AP, Jovin TM (2009) A triple-emission fluorescent probe reveals distinctive amyloid fibrillar polymorphism of wild-type alpha-synuclein and its familial Parkinson's disease mutants. Biochemistry 11;48(31):7465–7472
13. Jimenez JL, Guijarro JI, Orlova E, Zurdo J, Dobson CM, Sunde M, Saibil HR (1999) Cryo-electron microscopy structure of an SH3 amyloid fibril and model of the molecular packing. EMBO J 18(4):815–821
14. Kirschner DA, Abraham C, Selkoe DJ (1986) X-ray diffraction from intraneuronal paired helical filaments and extraneuronal amyloid fibers in Alzheimer disease indicates cross-β conformation. Proc Natl Acad Sci USA 83(2):503–507
15. Braak H, Braak E, Grundkeiqbal I, Iqbal K (1986) Occurrence of neuropil threads in the senile human-brain and in Alzheimers-disease—a 3 rd location of paired helical filaments outside of neurofibrillary tangles and neuritic plaques. Neurosci Lett 65 (3):351–355
16. Reusche E, Ogomori K, Diabold J, Johannisson R (1992) Electron-microscopic study of paired helical filaments and cerebral amyloid using a novel en-bloc silver staining method. Virchows Arch, A Pathol Anat Histopathol 420(6):519–525
17. Ferrari A, Hoerndli F, Baechi T, Nitsch RM, Götz J (2003) Beta-amyloid induces paired helical filament-like tau filaments in tissue culture. J Biol Chem 278(41):40162–40168
18. Crowther RA (1991) Straight and paired helical filaments in Alzheimer-disease have a common structural unit. Proc Natl Acad Sci USA 88(6):2288–2292
19. Inoue S, Kuroiwa M, Kisilevsky R (2002) AA protein in experimental murine AA amyloid fibrils: a high resolution ultrastructural and immunohistochemical study comparing aldehydfixes and cryofixed tissues. Amyloid 9(2):115–125
20. Makovitzky J, Richter S (2009) The relevance of the aldehyde bisulfite toluidine blue reaction and its variants in the submicroscopic carbohydrate research. Acta Histochem 111(4):273–291
21. Smith JF, Knowles TPJ, Dobson CM, MacPhee CE, Welland ME (2006) Characterization of the nanoscale properties of individual amyloid fibrils. Proc Natl Acad Sci USA 103(43):15806–15811
22. Dong M, Hovgaard MB, Mamdouh W, Xu S, Otzen DE, Besenbacher F (2008) AFM-based force spectroscopy measurements of mature amyloid fibrils of the peptide glucagons. Nanotechnology 19(38), article number: 384013
23. Porter AE, Knowles TPJ, Muller K, Meehan S, McGuire E, Skepper J, Welland ME, Dobson CM (2009) Imaging amyloid fibrils within cells using a Se-labelling strategy. J Mol Biol 392 (4):868–871
24. Ferguson N, Becker J, Tidow H, Tremmel S, Sharpe TD, Krause G, Flinders J, Petrovich M, Berriman J, Oschkinat H, Fersht AR (2006) General structural motifs of amyloid protofilaments. Proc Natl Acad Sci USA 103(44):16248–16253
25. Iwata K, Fujiwara T, Matsuki Y, Akutsu H, Takahashi S, Naiki H, Goto Y (2006) 3D structure of amyloid protofilaments of beta2-microglobulin fragment probed by solid-state NMR. Proc Natl Acad Sci USA 103(48):18119–18124
26. Celej MS, Jares-Erijman EA, Jovin TM (2008) Fluorescent N-arylaminonaphthalene sulfonate probes for amyloid aggregation of alpha-synuclein. Biophys J 94(12):4867–4879
27. Cathcart ES, Shirahama T, Cohen AS (1967) Isolation and identification of a plasma component of amyloid. Biochim Biophys Acta 147(2):392–393
28. Romhanyi G, Deak G, Fisher J (1975) Aldehyde bisulfite-toluidine blue (ABT) staining as a topo-optical reaction for demonstration of linear order of vicinal OH groups in biological structures. Histochemistry 43(4):333–348
29. Makovitzky J, Richter S, Appel TR (2006) Topooptical investigations and enzymatic digestions on tissue-isolated amyloid fibrils. Acta Histochem 108(3):193–196
30. Jin L-W, Claborn KA, Kurimoto M, Geday MA, Maezawa I, Sohraby F, Estrada M, Kaminksy W, Kahr B (2003) Imaging linear birefringence and dichroism in cerebral amyloid pathologies. Proc Natl Acad Sci USA 100(26):15294–15298
31. Finzi L, Bustamante C, Garab G, Juang CB (1989) Direct observation of large chiral domains in chloroplast thylakoid membranes by differential polarization microscopy. Proc Natl Acad Sci USA 86(22):8748–8752
32. Garab G, Pomozi I, Jörgens R, Weiss G (2005) Method and apparatus for determining the polarization properties of light emitted, reflected or transmitted by a material using a laser scanning microscope. US Patent 6(856):391
33. Steinbach G, Pomozi I, Zsiros O, Menczel L, Garab G (2009) Imaging anisotropy using differential polarization laser scanning confocal microscopy. Acta Histochem 111(4):317–326
34. Steinbach G, Pomozi I, Zsiros O, Pay A, Horváth GV, Garab G (2008) Imaging fluorescence detected linear dichroism of plant cell walls in laser scanning confocal microscope. Cytom A 73A(3):202–208
35. Steinbach G, Pomozi I, Garab G, Makovitzky J (2006) Periodic twisted structure of amyloid fibrils revealed by differential polarization laser scanning microscopy. FEBS J 273(suppl 1):65
36. Pras M, Schubert M, Zucker-Franklin D, Rimon A, Franklin EC (1968) The characterization of soluble amyloid prepared in water. J Clin Invest 47(4):924–933
37. Linke RP (1983) Senile cardiac amyloid: biochemical and immunohistochemical results. In: Platt D (ed) Cardiology and ageing. Ist International Erlangen-Nürnberg Symposium on Experimental Gerontology 20–23 October 1982. Schattauer Verlag, Stuttgart, pp 81–97
38. Scherzinger E, Lurz R, Turmaine M, Mangiarini L, Hollenbach B, Hasenbank R, Bates GP, Davies SW, Lehrach H, Wanker EE (1997) Huntington-encoded polyglutamine expansions form amyloid-like protein aggregates in vitro and in vivo. Cell 90(3):549–558
39. Appel TR, Richter S, Linke RP, Makovitzky J (2005) Histochemical and topo-optical investigations on tissue-isolated and in vitro amyloid fibril. Amyloid 12(3):174–183
40. Romhányi G (1979) Selektive Darstellung sowie methodologische Möglichkeiten der Analyse ultrastruktureller Unterschiede von Amyloidablagerungen. Zentralbl Allg Pathol 123:9–16
41. Romhanyi G (1958) Submicroscopic structure of elastic fibres as observed in the polarization microscope. Nature 182(4640):929–930
42. Garab G, van Amerongen H (2009) Linear and circular dichroism in photosynthesis research. Photosynth Res 101(2–3):135–146
43. Khurana R, Uversky VN, Nielsen L, Fink AL (2001) Is Congo Red an amyloid-specific dye? J Biol Chem 276(25):22715–22721
44. Szito T, Garab G, Mustárdy LA, Kiss JG, Faludi-Dániel A (1984) Increasing fluctuation in orientation of pigment protein complexes within photosynthetic membranes treated with linolenic acid. Photobiochem Photobiophys 8(4):239–249

45. Tinoco IJ, Mickols W, Maestre MF, Bustamante C (1987) Absorption, scattering, and imaging of biomolecular structures with polarized-light. Ann Rev Biophys 16:319–349
46. Keller D, Bustamante C (1986) Theory of the interaction of light with large inhomogeneous molecular aggregates. II. Psi-type circular dichroism. J Chem Phys 84:2972–2979
47. Chirico G, Langowski J (1996) Brownian dynamics simulations of supercoiled DNA with bent sequences. Biophys J 71(2):955–971
48. Bishop TC (2008) Geometry of the nucleosomal DNA superhelix. Biophys J 95(3):1007–1017
49. Bondarenko VA, Jiang YI, Studitsky VM (2003) Rationally designed insulator-like elements can block enhancer action in vitro. EMBO J 22:4728–4737
50. Kaminsky W, Jin L-W, Powell S, Maezawa I, Clabon K, Branham C, Kahr B (2006) Polarimetric imaging of amyloid. Micron 37 (4):324–338